Phase-transition behavior of a hard-core lattice gas with a tricritical point

Mark W. Springgate and Douglas Poland
Department of Chemistry, The Johns Hopkins University, Baltimore, Maryland 21218
(Received 10 July 1978)

The phase-transition behavior of a hard-core lattice gas with nearest-neighbor exclusion and next-nearest-neighbor attraction on the plane-square lattice has been determined using high- and low-density activity series including double series in the sublattice activities reported here. The model exhibits a line of second-order transition points at high temperature and a line of first-order transition points at low temperature intersecting at a tricritical point. The series for the various thermodynamic functions do not converge equally well at all temperatures, requiring the utilization of a strict criterion (outlined here) for assessing the reliability of numerical results. From the combined behavior of the thermodynamic functions we have determined the radius of convergence of the series at all temperatures, the position of the singularities (in terms of the fugacity) on the real axis approaching the intersection of the unit circle at low temperature. Along the second-order line the critical exponents are estimated to be $\alpha \simeq 0.0$ (logarithmic singularity), $\beta \simeq 1/8$, and $\gamma \simeq 7/4$. At the tricritical point $\alpha_t \simeq 1$ and $\gamma_t \simeq 1$ are in agreement with the ϵ-expansion results of Stephens and McCauley for $d = 2$. The density series are poorly behaved, and we can only estimate the phase diagram.

I. INTRODUCTION

In a previous paper[1] we reported the high- and low-density activity series through 11 terms for the plane-square lattice gas with nearest-neighbor exclusion and next-nearest-neighbor attraction. The model is illustrated in Figs. 1 and 2 and compared with the plane-square Ising model. Figure 1(a) illustrates the Ising model where, given a particle at a lattice site (solid dot), there is an attractive interaction if another particle is on a neighboring lattice site (these sites being shown by the open circles) there being no interaction if two particles are separated by more than a single lattice spacing. The model we are treating is illustrated in Fig. 1(b): given a particle (solid dot) at a lattice site, no particle can occupy the nearest-neighbor sites (indicated by ×'s) but there is an attractive interaction between particles on next-nearest-neighbor sites (indicated by open circles). The model can also be viewed in a slightly different fashion. Given the Ising model as illustrated in Fig. 2(a), the present model is obtained if one subdivides the space further and introduces a new lattice (which we call the B sublattice, the original being the A sublattice) shown by dotted lines in Fig. 2(b). In this view particles exclusively on the A sublattice or exclusively on the B sublattice behave exactly as in the Ising model with nearest-neighbor attraction (nearest neighbor with respect to a particular sublattice). In general for particles

FIG. 1. (a) Schematic illustration of the two-dimensional Ising model; a particle at the site indicated by the solid circles interacts only with particles on the sites indicated by open circles. (b) Schematic illustration of the present model; given a particle at the site indicated by the solid circle, no particles are allowed at the sites indicated by ×'s while the central particle interacts between particles at the sites indicated by open circles.

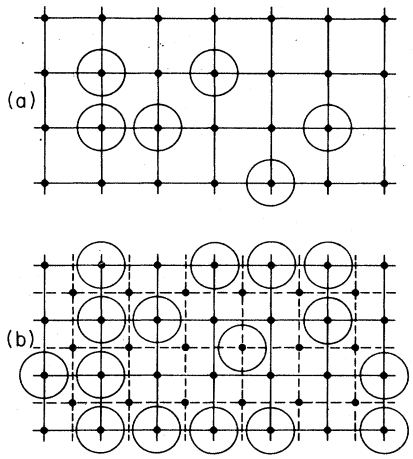

FIG. 2. (a) Schematic illustration of a configuration of particles on the plane-square lattice for the Ising model. (b) Schematic illustration of a configuration of particles for the present model. In addition to the lattice of 2(a) (solid lines) there is an additional set of lattice points representing a sublattice (dashed lines).

both on the A and B sublattices, there is no attraction between particles on different sublattices, but there is exclusion between nearest-neighbor A-B sites. The essential difference between the present model and the Ising model is that in the limit of close packing all the particles must either be on the A or the B sublattice (while at low density both are equally probable). Thus the present model contains a long-range ordering tendency not found in the Ising model.

Since this model is the simplest lattice analog of a gas that takes into account both the repulsive and attractive parts of the potential, the phase-transition behavior of the model is of some interest. In the present paper we report new double series in the sublattice activities for this model and present an analysis of the activity series using Padé approximants and the ratio method.

In the high-temperature limit, in which one has just the nearest-neighbor repulsion, the present model has been discussed by a number of workers. Domb discussed the model in connection with the theory of melting.[2] Approximate treatments have been given by Temperly[3] using the Bethe approximation, Burley[4] using exact and approximate series expansions, Levesque and Verlet[5] and Jancovici and Stell[6] using the Percus-Yevick and hypernetted chain integral equations, and Kaye and Burley[7] using a Kikuchi approximation. The results of these approximate methods range from a result of no transition[5] to a first-order transition.[7] Runnels and Combs,[8] Ree and Chesnut,[9] and Nisbet and Farquhar[10] calculated exact properties for finite strips of lattice and extrapolated the results to the thermodynamic limit, their results agreeing very well with the series results of Gaunt and Fisher.[11] Gaunt and Fisher found a second-order or continuous transition at $z=3.76$ (z the activity) with no discontinuity in density between the coexisting phases at the phase-transition point. The only completely rigorous result for the model is the work of Dobrusin[12] who proves using a modified Peierls argument that a phase transition must exist of the kind found by Gaunt and Fisher.[11]

The present model was first treated at all temperatures by Runnels, Salvant, and Streiffer[13] who extrapolated exact numerical results for finite lattice strips to the thermodynamic limit. Kaye and Burley,[14] using a Kikuchi approximation, came to the same results as Runnels *et al.* although their values for the transition parameters differ greatly. The essential conclusion of the two works is the same. Above a characteristic temperature a line of second-order or continuous phase-transition points separates an ordered and disordered phase, the transition point marking the beginning of a difference in sublattice densities for the ordered phase; below the characteristic temperature a line of first-order phase-transition points separates the ordered and disordered phases which differ both in the sublattice density and normal density. The temperature at which the line of second-order transitions meets the line of first-order transitions is known in the literature as a tricritical point (TCP).

These studies leave a number of important questions unanswered concerning the nature of the first- and second-order phase transitions, how the various thermodynamic quantities behave along the line of phase-transition points, and what happens at the tricritical point where the line of second-order phase-transition points joins the line of first-order phase-transition points.

In Sec. II we define the activity series for the various thermodynamic functions we will examine and define the appropriate critical exponents required to describe the singularities in these quantities along the second-order line and at the tricritical point. We then briefly review the analysis of the high-temperature limit for the present model given by Gaunt and Fisher[11] and the two-dimensional Ising model in the neighborhood of the critical point, using these two cases to illustrate difficulties in the analysis of activity series. We propose a method for testing the reliability of results obtained from extrapolation of the series using the ratio method. Using this criterion for accepting and rejecting numerical results, we report the radius of convergence of both the low- and high-density activity series as a function of temperature, and the critical exponents at selected temperatures along the second-order line and at the tricritical point. Unfortunately the corresponding series in the density are poorly behaved and we are not able to determine the phase diagram from the radius of convergence of the density series. We do give an approximate phase diagram based on the extrapolation of activity series. We conclude with a discussion of the phase-transition behavior.

II. SERIES EXPANSIONS

In the present section we outline the series expansions we will use and define symbols.

A. Activity series

In a previous paper[1] we reported the coefficients b_n and b_n' through $n=11$ for the series ($\beta=1/kT$, p is the pressure, and z is the activity)

$$\beta p=\sum_n b_n z^n \quad \text{(low density)} \tag{1a}$$

$$2\beta p=-\ln(z'x^2)+\sum_n b'_n z'^n \quad \text{(high density)} \tag{1b}$$

where b_n and b'_n are finite polynomials in the interaction parameter x (where ϵ is the interaction energy)

$$x=e^{-\beta\epsilon} \tag{2}$$

and

$$z'=1/zx^4 . \tag{3}$$

As was mentioned in the Introduction and illustrated in Fig. 2(b), the present model can be viewed as consisting of an A and B sublattice. Introducing activities z_a and z_b for particles, respectively, on the A and B sublattices, then βp can be represented as a double series in z_a and z_b (which can be thought of simply as labels indicating whether a particle is on the A or B sublattice). In the Appendix high- and low-density series in the sublattice activities are given for the present model; these series have been calculated using the Toeplitz matrix technique of Springgate and Poland.[1] The high- and low-density series are (for low density)

$$\beta p=\sum_n\sum_m b_{mn} z_a^{n-m} z_b^m \tag{4a}$$

(for high density)

$$2\beta p=-\ln(z'_a x^2)+\sum_n\sum_m b'_{mn}(z'_a)^{n+m}(z'_b)^{-m}, \tag{4b}$$

where

$$z'_a=1/z_a x^4, \quad z'_b=1/z_b x^4 . \tag{5}$$

We have obtained the b_{mn} through $n=9$ and the b'_{mn} through $n=8$.

B. Fugacity series

It is useful to introduce the fugacity

$$y=zx^2 \tag{6}$$

since in the plane-square Ising model the phase transition occurs at $y=1$. The low-density series for the pressure then becomes

$$\beta p=\sum_n c_n y^n , \tag{7}$$

where

$$c_n=b_n/x^{2n} . \tag{8}$$

Defining

$$y'=1/zx^2=z'x^2 , \tag{9}$$

the high-density series for the pressure is given by

$$2\beta p=-\ln y'+\sum_n c'_n y'^n , \tag{10}$$

where

$$c'_n=b'_n/x^{2n} . \tag{11}$$

One can also define sublattice fugacities in analogy with Eqs. (6) and (9) giving, for example, for the low-density series for the pressure

$$\beta p=\sum_n\sum_m c_{mn} y_a^{n-m} y_b^m \tag{12}$$

$$c_{mn}=b_{mn}/x^{2n} .$$

C. Thermodynamic functions

Given the low- and high-density activity series for the pressure one can obtain activity series for other thermodynamic functions by use of standard thermodynamic relations. Below we list the thermodynamic functions that we will use giving the series for the low-density expansions. Pressure:

$$\Gamma=\beta p=\sum_n b_n z^n . \tag{13}$$

Density:

$$\rho=\frac{\partial\Gamma}{\partial\ln z}=\sum_n n b_n z^n . \tag{14}$$

Sublattice densities:

$$\rho_a=\frac{\partial\Gamma}{\partial\ln z_a}=\sum_{n,m}(n-m)b_{mn} z_a^{n-m} z_b^m , \tag{15a}$$

$$\rho_b=\frac{\partial\Gamma}{\partial\ln z_b}=\sum_{n,m} m b_{mn} z_a^{n-m} z_b^m . \tag{15b}$$

Long-range order parameter:

$$R=2(\rho_a-\rho_b) . \tag{16}$$

Modified isothermal compressibility:

$$\chi=\frac{\partial^2\Gamma}{\partial(\ln z)^2}=\sum_n n^2 b_n z^n . \tag{17}$$

Staggered compressibility:

$$\chi^{\dagger}=(\partial/\partial\ln z_a-\partial/\partial\ln z_b)^2\Gamma . \tag{18}$$

The isothermal compressibility K_T is given by

$$K_T=\rho^{-1}\partial\rho/\partial\rho=\beta\chi/\rho^2 . \tag{19}$$

Since all the functions listed above are obtained by taking the logarithmic derivative with respect to z, the series in y have the same form. For example,

$$\Gamma=\sum_n c_n y^n,$$
$$\rho=\sum_n c_n y^n, \tag{20}$$
$$\chi=\sum_n n^2 c_n y^n.$$

D. Density series

From Eq. (14) one has ρ as a series in z. On inverting the series one obtains

$$z=\sum_n a_n \rho^n \tag{21}$$

with analogous equations in terms of the sublattice activities and densities. Using Eq. (21) in Eq. (13), for example, yields the virial expansion for the pressure

$$\Gamma=\sum_n B_n \rho^n \tag{22}$$

with similar expansions for χ, R, and $\chi^\dagger$.

E. Critical and tricritical point exponents

Along the second-order line and at the TCP the thermodynamic functions will diverge with characteristic exponents. In this paper we will follow the notation of Griffiths[15] and use the following definitions for these exponents. Let z_σ be the position of the singularity on the real positive z axis for the low-density activity series. Then along the second-order line we take

$$\chi(z)\sim K_T(z)\sim (z_\sigma - z)^{-\alpha},$$
$$R(z)\sim (z_\sigma - z)^{\beta}, \tag{23}$$
$$\chi^\dagger(z)\sim (z_\sigma - z)^{-\gamma}.$$

We will use a subscript t (i.e., $\alpha_t, \beta_t, \gamma_t$) to distinguish the exponents at the TCP from those along the second-order line. We will use a prime [as in Eq. (3)] to indicate high-density series; thus z_σ' is the position of the singularity on the positive z' axis for the high-density activity series with the exponents defined as α', β', and γ'. The nature of the singularity of course remains the same when one expresses the thermodynamic functions as fugacity series.

III. REVIEW OF THE BEHAVIOR OF ACTIVITY SERIES

Based on the previous work on the present model outlined in Sec. I we expect that there will be a transition of some kind at all temperatures (first order at low temperatures, second order at high temperatures with a tricritical point marking the change in order). Thus in the complex-z plane we expect a singularity of some kind on the real positive axis at all temperatures; we designate the position of the singularity by z_σ (or in terms of the fugacity, y_σ).

A. Numerical techniques

Letting $S(z)$ be any of the activity series [Eqs. (13)–(18)], then if $S(z)$ has a singularity of the form

$$S(z)=\sum_n A_n z^n \sim (z_\sigma - z)^{-\nu} \tag{24}$$

there are several techniques[16] to determine ν and z_σ given a finite number of the coefficients A_n. Domb and Sykes[17] have shown that for a singularity of the type shown in Eq. (24) the ratios successive terms should behave as

$$r_n = A_n/A_{n-1} = z_\sigma^{-1}[1+(\nu-1)/n] \tag{25}$$

yielding z_σ^{-1} as the intercept and $(\nu-1)/z_\sigma$ as the slope when r_n is plotted versus $1/n$. If a singularity other than that at z_σ determines the radius of convergence, then often a Euler transform can be found that maps the z plane such that the singularity on the real positive axis, z_σ, determines the radius of convergence. Alternatively one can use the technique of Padé approximants introduced by Baker *et al.*,[18] applying the technique to the logarithmic derivative of $S(z)$

$$\ln S(z)' = \partial \ln S(z)/\partial \ln z \sim \nu/(z_\sigma - z) \tag{26}$$

yielding z_σ as a simple pole on the real axis and ν as the residue of that pole (throughout this paper a prime indicates the logarithmic derivative).

Most of the work on obtaining critical exponents from series expansions have utilized series in β or functions of β (high-temperature series).[16] The reason for this is twofold: activity series are in general both more difficult to obtain and analyze than high-temperature series. Thus before presenting our analysis of the activity series for the present model, we review briefly the analysis of Gaunt and Fisher of the activity series for the high-temperature limit of the present model and also the behavior of the activity series for the Ising model in the neighborhood of the critical point.

B. High-temperature limit

Gaunt and Fisher[11] analyzed the activity series for the present model for the special case of

infinite temperature ($x=1$) in which case the model reduces to that of hard particles with nearest-neighbor exclusion. They utilized activity and density series and series based on the following Euler transforms:

$$u_z = z/(1+z)\,, \tag{27a}$$

$$u_\rho = \rho/(1+\rho)\,. \tag{27b}$$

For the low-density series they found that for all of the $S(z)$ the coefficients alternate in sign and increase in magnitude indicating that the radius of convergence is determined by a nonphysical singularity on the negative real axis which we designate as $z_\sigma^{(-)}$. From a study of Padé approximants to $\rho(z)$ and $\chi(z)$ Gaunt and Fisher found

$$z_\sigma^{(-)} = -0.1194 \pm 2 \tag{28}$$

which is apparently a branch point (as evidenced by the alternation of poles and zeros on the negative axis). This singularity dominates the behavior of all the $S(z)$ series. Padé approximants to $\chi^\dagger(u_z)$ and $\beta p(u_z)$ were able to pick up a singularity on the real positive axis giving

$$z_\sigma = 3.76 \pm 3\,. \tag{29}$$

Application of the ratio method to $\chi^\dagger(\rho)$ yielded

$$\rho_\sigma = 0.368 \pm 17\,. \tag{30}$$

From numerical calculations of the isotherm Gaunt and Fisher concluded that K_T remains finite at ρ_σ, although they could not rule out the possibility of a logarithmic singularity.

The ratio method applied to the high-density series gave a singularity on the negative real axis ($z_\sigma^{(-)} \simeq -3.8$) which dominates the behavior of the series. The behavior of poles obtained from Padé approximants applied to χ and $\chi^\dagger$ were not very regular but indicated a singularity on the real positive axis at $z_\sigma \simeq 3.80$ in agreement with that found from the low-density activity series [Eq. (29)]. Padé approximants applied to R gave $\beta = 0.12 \pm 2$; Gaunt and Fisher conjectured that $\beta = 0.125 = \frac{1}{8}$ exactly. Gaunt and Fisher found that the ratio method worked fairly well for R and $\chi^\dagger$ when the series were expressed in terms of u_z' [Eq. (27a) utilizing z'].

In summary, Gaunt and Fisher were able to determine z_σ, ρ_σ, and the exponent β. In general, the activity and density series were poorly behaved, the series being dominated by singularities on the negative real axis close to the origin. The series that proved most useful were $\chi^\dagger$ and R, both of these functions being derived from the double series in the sublattice activities [Eq. (4)] (it is for this reason that we calculated the double series for this model as a function of temperature).

C. Ising model near the critical point

In the previous subsection we reviewed the behavior of the activity series in the high-temperature limit, indicating that the analysis was difficult because of a singularity close to the origin on the negative real axis. At low temperature, at or below the TCP, one would expect the present model to behave in a fashion similar to the Ising model, the effect of the next-nearest-neighbor attractions being more important than the hard-core exclusive at low temperatures.

The curve marked (a) in Fig. 3 shows the ratios r_n as a function of $1/n$ for $\chi(y)$ for the two-dimensional Ising model (using through r_8) evaluated at the critical point ($x_c = [1/(\sqrt{2}-1)]^2 = 5.282\ldots$). In the Ising model the singularity occurs at $y_\sigma = 1$ (all the roots of the grand partition function being on the unit circle); the ratios are seen to oscillate, the oscillations becoming smaller as $1/n \to 0$, r_n approaching $y_\sigma^{-1} = 1$. Utilizing the Euler transform

$$u = y/(1+\phi y) \tag{31}$$

the curve marked (b) in Fig. 3 shows the ratios for $\chi(y, \phi)$ with $\phi = 0.5$ [the quantities shown are $r_n' = r_n - \phi$; see Eq. (44)]. The ratios no longer oscillate and form a smooth curve that extrapolates to $y_\sigma^{-1} = 1$ with slope slightly less than zero (in fact for $\chi(y)$, $\nu = \frac{14}{15}$ giving a slope of $-\frac{1}{15}$). Figure 3 thus illustrates the utility of the Euler transform in analyzing ratios.

While in the Ising model one knows exactly the value of x_c, in the present model we do not know the value of x_{TCP}. With this in mind we examined

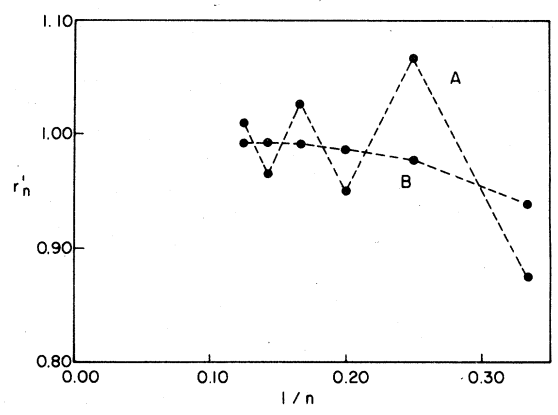

FIG. 3. Ratios r_n' for $\chi(y, \phi)$ for the two-dimensional Ising model at the critical point. Curve (a) is for $\phi = 0.0$ (no Euler transform) while curve (b) is for $\phi = 5$. The ratios are shown through $n = 8$.

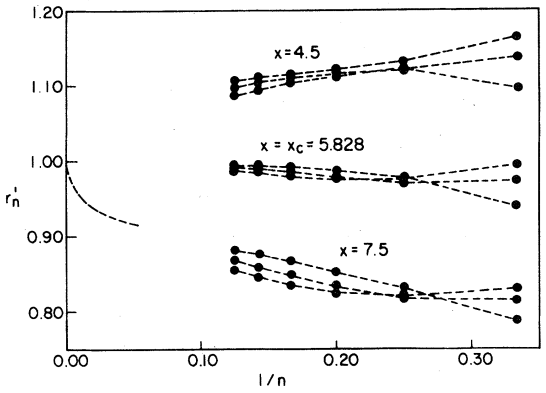

FIG. 4. Ratios r_n' for $\chi(y,\phi)$ for the two-dimensional Ising model for $x<x_c$, $x=x_c$, and $x>x_c$; each set of curves is for $\phi=0.5$, 1.0, and 1.5. The dashed curve near $1/n=0$ is the behavior of the ratios predicted by the driplet model of Fisher for $x>x_c$ (essential singularity). The ratios are shown through $n=8$.

the ratios for the Ising model above and below x_c to see if there was a characteristic pattern that might help in recognizing x_{TCP}. Figure 4 shows $r_n'=r_n-\phi$ for $\chi(y,\phi)$ for $\phi=0.5$, 1.0, and 1.5 for $x=4.5$, $x=x_c$, and $x=7.5$. All of the ratios vary smoothly and if the curves are interpreted using Eq. (42b) (to be discussed shortly) one finds apparent values of y_σ and ν that vary with x (temperature); in particular one finds $y_\sigma<1$ for $x<x_c$ ($T>T_c$) and $y_\sigma>1$ for $x>x_c$ ($T<T_c$). In fact for $T>T_c$ there no longer is a singularity on the real positive axis and for $T<T_c$ the singularity is at $y_\sigma=1$. The analysis by Fisher[19] of the droplet model supports the conjecture that below T_c the singularity is an essential one. For an essential singularity of the sort predicted by the droplet model the ratios behave like the dotted line in Fig. 4, the curve hooking into $y_\sigma=1$ with an infinite slope.

The curves in Fig. 4 for the Ising model indicate that even though the ratios appear to extrapolate smoothly, one can be greatly misled as to the true value of y_σ and ν if one is in fact at a temperature below the TCP (in the present model a singularity persists on the real positive axis up to infinite temperature, unlike the case of the Ising model). The diagnostics for being at a temperature below T_c seem to be that the apparent value of $y_\sigma(T)$ increases as the temperature decreases and the ratios do not converge well with respect to the value of ϕ used in the Euler transform of Eq. (31) (they appear to "float" one above the other).

IV. ANALYSIS OF ACTIVITY SERIES

In our first attempt to analyze the activity series for the present model we ran into a number of problems. At high temperature the behavior of the series is dominated by nonphysical singularities, and while the use of the Euler transform often improved the behavior, the results (y_σ and ν) often were found to be strong functions of the parameter ϕ used in Eq. (31). In addition the different $S(y)$ did not always give the same y_σ and ν, and y_σ and ν were found to vary with temperature in a nonmonotonic fashion. It was thus clear that the series were not equally well converged at all temperatures and that it was essential to develop a test for reliability. We begin by describing the criterion we used.

A. Criterion for convergence

As is illustrated by the work of Gaunt and Fisher and the ratios for the Ising model given in Fig. 4, it is necessary to utilize a transformation of variable such as the Euler transform of Eq. (31) to obtain information from activity series. To proceed it is necessary to analyze the nature of the Euler transform in more detail.

Consider the series

$$S(y)=A_0+\sum_{n=1}^{\infty}A_n y^n . \tag{32}$$

Introducing the transformation

$$u=y/(1+\phi y) \tag{33}$$

with the inverse transformation

$$y=u/(1-\phi u) \tag{34}$$

one then has for $S(u)$

$$S(u)=A_0+\sum_{n=1}^{\infty}B_n u^n , \tag{35}$$

where

$$B_n=\sum_{k=0}^{n-1}\phi^k\binom{n-1}{k}A_{n-k} . \tag{36}$$

If

$$S(y)=[1/(1-y/y_\sigma)]^\nu \tag{37}$$

then

$$A_n=A_n' y_\sigma^{-n} , \tag{38}$$

$$A_n'=\nu(\nu+1)\cdots(\nu+n-1)/n! ,$$

and

$$S(u)=\left(\frac{1-\phi u}{y_\sigma[1-u(y_\sigma^{-1}+\phi)]}\right)^\nu . \tag{39}$$

For the A_n of Eq. (38), the ratios for $S(u)$ are

$$r_n=\frac{B_n}{B_{n-1}}=y_\sigma^{-1}\left[\sum_{k=0}^{n-1}(\phi y_\sigma)^k\binom{n-1}{k}A'_{n-k}(\nu)\right]\times\left[\sum_{k=0}^{n-2}(\phi y_\sigma)^k\binom{n-2}{k}A'_{n-k-1}(\nu)\right]^{-1}. \quad (40)$$

For the case of $\phi=0$, $S(y)=S(u)$ and

$$r_n=y_\sigma^{-1}[1+(\nu-1)/n] \quad (41)$$

as noted previously [Eq. (25)].

As $u\to u_\sigma$, where $u_\sigma=y_\sigma/(1+\phi y_\sigma)$, then one has the asymptotic relations

$$S(u)\sim\left(\frac{1}{1-u/u_\sigma}\right)^\nu=\left(\frac{1}{1-u(y_\sigma^{-1}+\phi)}\right)^\nu, \quad (42a)$$

$$r_n\sim(y_\sigma^{-1}+\phi)[1+(\nu-1)/n]. \quad (42b)$$

One of the problems of using the Euler transform is apparent in Eq. (40): while r_n is a function of the unknowns y_σ and ν, it is a complicated function. In principle, two values of r_n are sufficient information to calculate y_σ and ν; one could then extrapolate the values obtained from pairs, e.g., r_n and r_{n-1}, as a function of $1/n$ but this is a troublesome procedure since one has to scan a space of two variables. In general the ratios for $S(u)$ do not give a straight line when plotted versus $1/n$. From Eq. (42b) the ratios are asymptotic to a straight line from which y_σ can be calculated from the intercept and ν from the slope. However, to use Eq. (42b) one must have enough terms in the series to estimate the limiting behavior.

For special values of ν, Eq. (40) simplifies considerably. For $\nu=0$, 1, and 2 one has for $\nu=0$ (logarithmic singularity)

$$r_n=(y_\sigma^{-1}+\phi)(1-1/n)\left(\frac{1-b^n}{1-b^{n-1}}\right);\quad b=\frac{\phi y_\sigma}{1+\sigma y_\sigma}; \quad (43a)$$

for $\nu=1$

$$r_n=(y_\sigma^{-1}+\phi); \quad (43b)$$

for $\nu=2$

$$r_n=(y_\sigma^{-1}+\phi)\left(1+\frac{1}{n(1+2\phi y_\sigma/n)}\right). \quad (43c)$$

In particular for $\nu=1$ [in which case $S(y)$ has a simple pole at $y=y_0$] the ratios of $S(u)$ are independent of n. If one forms

$$r'_n=r_n-\phi \quad (44)$$

then for $\nu=1$ the ratios are independent of n and independent of ϕ giving a straight line pointing directly (with zero slope) at y_σ^{-1} as $1/n\to 0$.

Based on the above properties of the series $S(u)$ we have devised the following scheme to determine y_σ and ν and to assess the reliability of the calculation. The scheme involves the following steps:

(i) One makes an initial estimate of ν, either from Eq. (42b), Padé approximants [using Eq. (26)], or from theoretical notions concerning the values of the exponents.

(ii) One then forms the series

$$S_1(u)=[S(u)]^{1/\nu}\sim[1/(1-u/u_\sigma)]. \quad (45)$$

The ratios, r'_n of Eq. (44), for the function $S_1(u)$ should be independent of both of ϕ and n.

(iii) One further forms the series

$$S_2(u)=[S(u)']^{1/\nu}\sim[1/(1-u/u_\sigma)]^{(\nu+1)/\nu}. \quad (46)$$

The ratios r'_n for the function $S_2(u)$ should be functions both of n and ϕ and should converge to y_σ^{-1} as $1/n\to 0$ according to Eq. (43c) [using Eq. (44)].

(iv) If the initial estimate of ν does not lead to the properties of S_1 and S_2 given, respectively, in (ii) and (iii) above, one either tries another value of ν or rejects the series as being poorly converged at the temperature in question.

The essential feature of the above scheme is the use of at least three values of the parameter ϕ in the Euler transform to give $S(u)$. For a single value of ϕ one often obtains smoothly varying ratios that give grossly incorrect values of y_σ and ν (we will discuss an example shortly in connection with Fig. 10). In order to trust the results of ratio plots, $S_1(u)$ must be independent of ϕ and $S_2(u)$ must give converging ratios.

The use of this scheme is illustrated in Fig. 5 where the ratios are given for the high-density modified compressibility $\chi(y',\phi)$ (derived from the

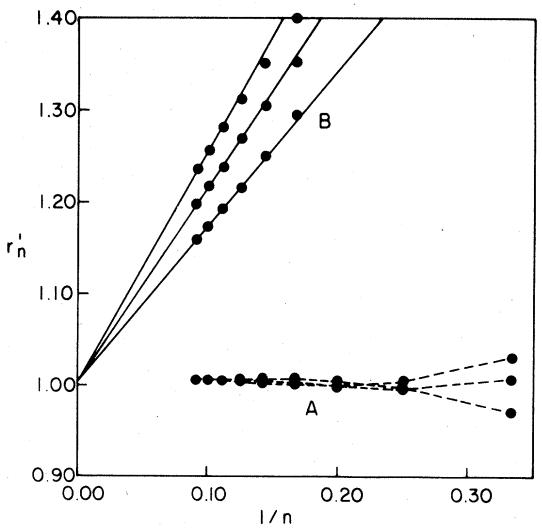

FIG. 5. Ratios r'_n at $x=6.0$ for (a) $[\chi(y',\phi)]^{15/14}$; (b) $[\chi(y',\phi)']^{15/14}$. Each set of curves is for $\phi=0.5$, 1.0, and 1.5. The ratios are shown through $n=11$.

11-term z' series for βp). Since at low temperature one might expect the behavior to be similar to that for the Ising model, we make the initial guess that the exponent is $\frac{14}{15}$. Figure 5 shows the ratios r_n' for the two functions

$$S_1=[\chi(y',\phi)]^{15/14},\quad S_2=[\chi(y',\phi)']^{15/14}, \tag{47}$$

from $\phi=0.5$, 1.0, and 1.5 at $x=6.0$. The ratios for S_1 are seen to be independent of n and ϕ giving a straight line of zero slope. The ratios for S_2 are functions of n and ϕ and give a set of three straight lines that converge to the same intercept as S_1. As we will discuss in Sec. VI, it is not clear whether the exponent for $\chi(y')$ is $\frac{14}{15}$ or 1.0. But clearly the exponent is very close to 1 and the ratios for both S_1 and S_2 clearly point to the same intercept y_c^{-1}. If one uses only S_1 one frequently has slight undulations in the ratios; any uncertainties in the horizontal extrapolation of the ratios for S_1 are greatly lessened by having the converging set of straight lines for S_2 pointing to the same intercept. If, as is frequently the case, the $r_n'(\phi)$ for S_2 do not give a set of curves that converge to a single y_c^{-1}, but rather give a set of three parallel lines, one can make no reasonable estimate of y_c and ν and must conclude that the series at this particular temperature are not well converged.

In Sec. IV B we will give several examples of ratios failing to converge well at certain temperatures that illustrate our criterion of accepting and rejecting results. In general throughout the rest of this paper we will use the behavior as illustrated in Fig. 5 as the criterion for accepting the results of ratio plots: if $S_1(u)$ gives ratios that are independent of n and ϕ and if $S_2(u)$ gives ratios that converge to the same y_c^{-1}, we accept the values of ν and y_c as reliable. To avoid crowding in graphs, we will show only S_1 in the ratio plots to be given in Secs. V and VI; we emphasize that all of our estimates of y_c and ν have been obtained from ratios that have a behavior similar to that shown in Fig. 5.

Before beginning our discussion of the analysis of the series we point out that we do not know the value of x_{TCP}. From numerical extrapolations of high- and low-density isotherms for βp we believe $x_{\mathrm{TCP}}>3.7$ (this estimate will be discussed in Sec. V). From the study of all the thermodynamic functions, our educated estimate is that x_{TCP} probably lies in the range $x=4$ to $x=5$. Thus in the temperature range $x=1.0$ to $x=3.7$ we assume we are along the second-order line. For x in the range $x=4.0$ to $x=5.0$ we assume we are in the region of the TCP.

Of course we have evidence to support these assumptions, a portion of which will be given in the following discussion. The important point is that there is no dramatic change in the behavior for partial series over a small temperature range. This is illustrated by the ratios for the Ising model shown in Fig. 4 where the behavior (with respect to slope) of the ratios does not change qualitatively in the range $x=4.5$ to $x=7.5$ (with $x_c=5.828$).

B. Low-density activity series

At $x=1$ Gaunt and Fisher found a singularity on the negative real z axis at $z_c^{(-)}=y_c^{(-)}\simeq-0.12$ while the singularity of interest on the positive real z axis was at $z_c=y_c\simeq3.76$. The singularity at $z_c^{(-)}$ completely dominates the series at $x=1$ and Euler transforms using a wide range of values for ϕ do not significantly improve the ratios. For $x\sim4$, one finds that $y_c^{(-)}$ has moved close to -1 while y_c is now close to $+1$. In the neighborhood of $x\sim4$, the function of $\chi(y,\phi)$ gives very smoothly varying ratios for ϕ in the range 0.5 to 1.5. Figure 6 shows r_n' for $[\chi(y,\phi)]^{15/14}$ at $\phi=0.5$ and $\phi=1.0$ at several values of x. As with the high-density function $\chi(y',\phi)$ shown in Fig. 5, we anticipated that the low-density series $\chi(y,\phi)$ would behave like the Ising model at x_c and chose the exponent $\alpha_t=\frac{14}{15}$ as a trial value. At $x=4.5$ and $x=4.0$ the ratios become independent of n and ϕ as n is increased giving straight lines with approximately zero slope. As x is decreased

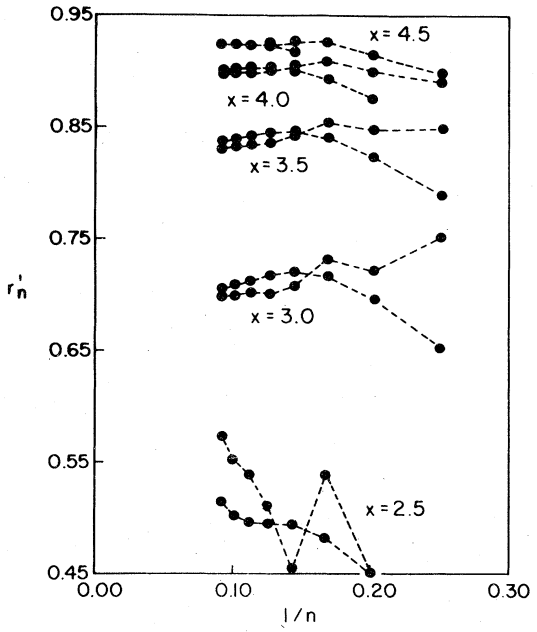

FIG. 6. Ratios r_n' at $x=4.5$, 4.0, 3.5, 3.0, and 2.5 for $\chi(y,\phi)^{15/15}$. Each pair of curves is for $\phi=0.5$ and 1.0. The ratios are shown through $n=11$.

from 3.5 to 2.5, the ratios become increasingly poorly behaved, the singularity on the negative real axis moving in toward the origin and dominating the behavior of the series as $x \to 1$. From the high-density series we will give evidence that $\alpha' \simeq 0$ (logarithmic singularity) along the second-order line. If $\alpha = \alpha'$, then α changes from $\alpha_t \simeq 1$ in the region of the TCP to $\alpha \simeq 0$ along the second-order line. The poor convergence of the ratios as x is decreased is presumably due to the change in the exponent; in general one will not see an abrupt change in the beginning terms of a series even though there is an abrupt change in the exponent. On the high-density side we will be able to follow the change in the ratios as a function of temperature in more detail.

Padé approximants to $\ln\chi(y,\phi)'$ and $\ln\chi(y,\phi)''$ substantiate the finding that $\alpha_t \simeq 1.0$ in the temperature range corresponding to $x \sim 4$ to 5. [The use in general of $\ln S''$ gives an additional estimate of the exponent: if $S \sim (y_\sigma - y)^{-\nu}$ then the residues of $\ln S'$ and $\ln S''$ for the pole $y = y_\sigma$ are ν and $\nu+1$, respectively, [see Eq. (27)]; throughout a prime indicates $\partial/\partial \ln y$.] For example, at $x=4.0$ and $x=4.5$ one obtains the following values of y_σ (with the corresponding residue given in parentheses) from the diagonal and off-diagonal approximants to the series $\ln\chi'$ and $\ln\chi''$ (with $\phi = 1.0$) for $x=4.0$

$$\ln\chi': 1.116\ (0.948), 1.123\ (0.981), 1.126\ (0.998);$$
$$\ln\chi'': 1.103\ (1.839), 1.142\ (2.151), 1.132\ (2.058). \quad (48)$$

for $x=4.5$

$$\ln\chi': 1.077\ (0.904), 1.078\ (0.912), 1.082\ (0.935);$$
$$\ln\chi'': 1.062\ (1.783), 1.090\ (2.025), 1.081\ (1.940).$$

Our best estimates of y_σ (calculated from averaging the values of y_σ obtained from approximants to $\ln\chi'$ and $\ln\chi''$ at several values of ϕ and from ratio plots) are $y_\sigma = 1.115$ at $x=4.0$ and $y_\sigma = 1.083$ at $x=4.5$. If one removes a pole at $y = y_\sigma$ from the approximants to $\ln\chi'$ and $\ln\chi''$ and calculates the residues, then using the above best estimates of y_σ one obtains the following estimates of α_t: for $x=4.0$

$$\ln\chi': \alpha_t = 0.957, 0.957, 0.956;$$
$$\ln\chi'': \alpha_t + 1 = 1.945, 1.944, 1.950; \quad (49)$$

for $x=4.5$

$$\ln\chi': \alpha_t = 1.031, 1.017, 1.010;$$
$$\ln\chi'': \alpha_t + 1 = 2.041, 2.033, 2.033.$$

The sets of data for a given value of x in (49) are internally quite consistent, giving $\alpha_t \simeq 0.95$ at $x=4.0$ and $\alpha_t \simeq 1.03$ at $x=4.5$. The problem is that we do not know the value of x_{TCP} and from the data given in the region $x=4.0$ to 4.5 there is no criterion for us to choose one value of x over another. For $x<4.0$, the ratios as shown in Fig. 6 are clearly increasingly poorly behaved, and do not give reliable estimates of y_σ and ν. For $x>5.5$ the ratios give a set of parallel lines similar to those shown in Fig. 4 for the Ising model for $x > x_c$ ($x=7.5$); in this temperature range the apparent values of y_σ vary with ϕ and show a general tendency to increase as the temperature is lowered. In this temperature region we conclude that $x > x_{\mathrm{TCP}}$ and as with the Ising model for $T < T_c$, the ratios are giving incorrect values of y_σ and α_t, probably because one has an essential singularity below x_{TCP}. Our conclusion is that the apparent temperature dependence of α_t shown in (49) is not real and arises for the same reason that the apparent value of α [obtained from applying Eq. (42b) to the data of Fig 4] for the Ising model varies with temperature in the neighborhood of x_c. From the data of (49), it is clear that if we knew $y_\sigma(x_{\mathrm{TCP}})$ accurately, we could obtain a very accurate estimate of α_t. Since we do not know x_{TCP} accurately, our best estimate is

$$\alpha_t = 1.00 \pm 0.05. \quad (50)$$

In general, if one has ratios that vary smoothly, as do those shown for $x=4.0$ and $x=4.5$ in Fig. 6 and those in Fig. 5, the Padé approximants also give consistent values of y_σ and ν such as those given in (48) and (49). We note the following technical point concerning Padé approximants that we observed in our calculations. If one calculates the residue for $\ln S'$ at the pole $y = y_\sigma$ as a function of ϕ, then the residue is invariant to ϕ for fixed y_σ for the diagonal approximant.

For $\chi^\dagger$ one finds that the ratios are well behaved only in the range $x \simeq 1.3$ to $x \simeq 1.8$. From Padé approximants, one finds $\gamma \simeq 1.6$ to 1.9; since this brackets the Ising model exponent 1.75, we make the initial estimate $\gamma = \frac{7}{4}$. In the range $x \simeq 1.3$ to 1.8 $[\chi^\dagger(y,\phi)]^{4/7}$ gives ratios that are approximately independent of n and ϕ. From Eqs. (17) and (18) one has the relation

$$\chi^\dagger = \chi - 4\chi_e^\dagger,$$
$$\chi_e^\dagger = \partial^2\Gamma/\partial \ln z_a \partial \ln z_b. \quad (51)$$

Following Gaunt and Fisher, we investigated $\chi_e^\dagger$ (the "essential" part of $\chi^\dagger$) with the hope that the interferring singularities in χ would be removed (from Fig. 6, the ratios for χ are poorly behaved above $x=4.0$). We find that in the range $x=2.0$ to 4.0, $\chi_e^\dagger$ indeed gives good ratios. Since

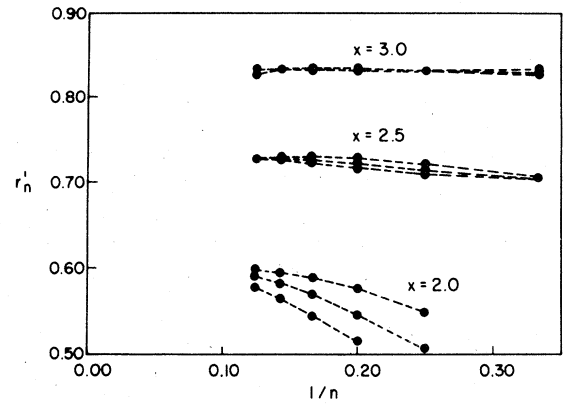

FIG. 7. Ratios r_n' at $x=3.0$, 2.5, and 2.0 for $[\chi_e^\dagger(y,\phi)]^{4/7}$. Each set of curves is for $\phi=1.5$, 2.0, and 2.5. The ratios are shown through $n=8$.

$\chi^\dagger$ and $\chi_e^\dagger$ have the same exponent γ, we use our estimate $\gamma=\frac{7}{4}$ and form the ratios for $[\chi_e(y,\phi)]^{4/7}$. These ratios r_n' are shown in Fig. 7 for $x=2.0$, 2.5, and 3.0 at $\phi=1.5$, 2.0, and 2.5 and clearly support the estimate $\gamma=\frac{7}{4}$. In particular, at $x=3.0$ the ratios are independent of n and ϕ to a degree that one cannot expect to exceed in this type of experimental mathematics; at $x=2.5$, the ratios are quite good, becoming independent of n and ϕ as n is increased; finally at $x=2.0$ one can infer from the behavior of the ratios at $x=2.5$ and $x=3.0$ that if one had more values of r_n', the ratios would converge to a limiting behavior that was independent of n and ϕ. But clearly, if one had just the ratios for $x=2.0$, the convergence would be in question as of course would be the values of y_σ and ν obtained therefrom. As with Fig. 6, Fig. 7 illustrates that at certain temperatures the ratios are very well converged, but that in general one systematically loses the convergence as the temperature is changed. Note in particular, that if one examined only the lower curve for $x=2.0$ (for a single value of ϕ) one would calculate quite incorrect values of y_σ and ν.

As mentioned previously, the ratios for $\chi^\dagger(y,\phi)$ support the results of Fig. 7 that $\gamma=\frac{7}{4}$ but only in the range $x\simeq 1.3$ to 1.8. At lower temperatures, in the region of the TCP ($x\sim 4$), $\chi^\dagger(y,\phi)$ again gives smoothly varying ratios. For $x>5$ the ratios for $\chi^\dagger(y,\phi)$ are independent of n and ϕ suggesting that the exponent γ_t is approximately unity. Padé approximants support the estimate $\gamma_t\simeq 1.0$. Below we give the residues obtained from the diagonal and off-diagonal Padé approximants to $\ln\chi^\dagger(y,\phi)'$ at $x=5.5$ and $x=6.0$. For $x=5.5$

$$\phi=0.5:\ \gamma_t=1.022, 1.020, 1.020;$$
$$\phi=1.0:\ \gamma_t=1.031, 1.020, 1.020;$$
$$\phi=1.5:\ \gamma_t=1.017, 1.020, 1.044.$$

For $x=6.0$ (52)

$$\phi=0.5:\ \gamma_t=1.006, 0.930, 0.937;$$
$$\phi=1.0:\ \gamma_t=1.107, 0.930, 0.930;$$
$$\phi=1.5:\ \gamma_t=0.835, 0.930, 1.133.$$

From $\chi(y,\phi)$ in the range $x=1.3$ to 1.8 and from $\chi_e^\dagger(y,\phi)$ in the range $x=2.0$ to 3.0 (see Fig. 7) we estimate that $\gamma=\frac{7}{4}$ along the second-order line. For x in the range 3.0 to 4.5 the ratios for $\chi^\dagger$ and $\chi_e^\dagger$ do not converge well and presumably this is due to the change in γ at $x_{\rm TCP}$. From (51) one sees that $\gamma_t\simeq 1$ for $x>5.0$ Since we expect $x_{\rm TCP}\sim 4$, the data of (52) are probably for $x>x_{\rm TCP}$ and one has the problem discussed in connection with Fig. 4 of the possibility that one is dealing with an essential singularity and that the apparent small drift with x of the exponent is due to this.

In summary, we obtain good convergence for the thermodynamic functions of interest in the following temperature ranges.

$$\chi:\ x\simeq 3.7 \text{ to } 5.0;$$
$$\chi^\dagger:\ x\simeq 1.3 \text{ to } 1.8; \quad (53)$$
$$\chi_e^\dagger:\ x\simeq 2.0 \text{ to } 3.9.$$

Fortunately, the ranges of x given in (53) collectively cover the range $x=1.3$ to 5.0. We thus have a good estimate of $y_\sigma(x)$ in the range $x=1.3$ to 5.0 [from Gaunt and Fisher[11] we have $y_\sigma(x=1)$]; the values of y_σ we accept are obtained from the extrapolation of ratios such as those for $\chi_e^\dagger$ at $x=3.0$ in Fig. 7 and are backed up by the values of y_σ obtained from Padé approximants [as illustrated in (48) and (49)]. For $x>5.0$ we have estimated $y_\sigma(x)$ from the intersection of $\beta p(y)$ and $\beta p(y')$ by simple curve fitting of the series; we will discuss this approach further in Sec. V.

Figure 8 shows $y_\sigma(x)$ as obtained collectively from the thermodynamic functions in the manner just discussed. We also show $y_\sigma^{(-)}$, the singularity closest to the origin on the negative real axis. From Fig. 8 one sees that $y_\sigma(x)$ drops from 3.76 at $x=1.0$ to $y_\sigma\sim 1$ rapidly as x is increased. Likewise $y_\sigma^{(-)}(x)$ moves from -0.12 at $x=1.0$, away from the origin, approaching -1 as x is increased. In Fig. 8, the lines $y_\sigma=+1$ and $y_\sigma^{(-)}=-1$ indicate the corresponding singularities in the Ising model (for $x<x_c$, there is no singularity on the real positive axis in the Ising model, this being indicated by a dashed line in Fig. 8). Thus clearly for the present model, the singularities in y on

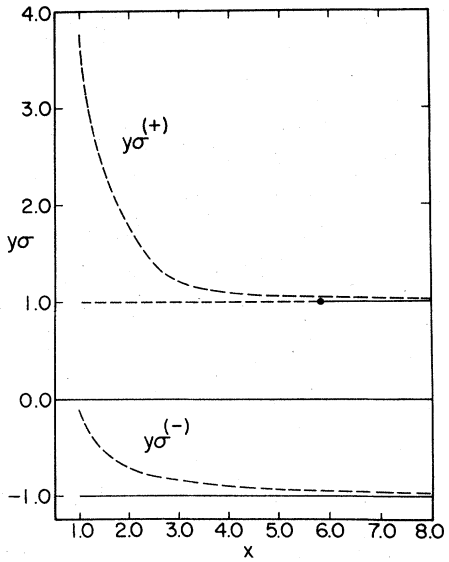

FIG. 8. Radius of convergence of the activity series expressed as the fugacity $y_\sigma = z_\sigma x^2$ as a function of x. The upper dashed curve shows y_σ, the position of the singularity on the real positive axis while the lower curve ($y_\sigma^{(-)}$) shows the position of the singularity closest to the origin on the negative real axis. The lines at +1 and −1 are the values of y and $y_\sigma^{(-)}$ for the two-dimensional Ising model; the dot indicates the Ising model critical point.

the real axis approach the intersection of the unit circle with the real axis rapidly as x is increased and in general the behavior of all the series becomes Ising-like for $x > 4.0$. Of course as $x \to 1$, the position of the singularities changes dramatically, becoming dominated by the hard core, a feature not present in the Ising model.

C. High-density activity series

The behavior of the high-density series is in general better than that of the low-density series. The reason for this is clear from the analysis of Gaunt and Fisher of the high-temperature ($x=1$) limit: the position of the singularity on the real positive z axis is the same (within the error of the numerical techniques) for both the high- and low-density activity series; however, for the low-density series the interfering singularity on the negative real axis was at $z_\sigma^{(-)} \simeq -0.12$, while the corresponding singularity for the high-density series was at $z_\sigma^{(-)} \simeq -z_\sigma \simeq -3.8$. This means that the singularity on the negative real axis has much less influence in the high-density series than in the low density series.

We will give a detailed analysis only for $\chi(y', \phi)$, the behavior of the other thermodynamic functions being much the same (with in general better convergence) as for the low-density series. Before discussing χ, we review the results obtained

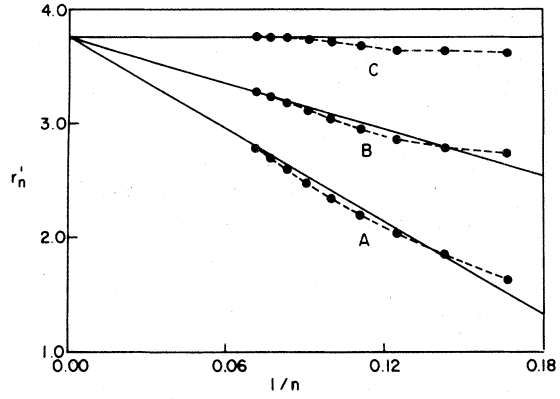

FIG. 9. Ratios r'_n at $x=1.0$ and $\phi=3.0$ for (a) $\rho(y')$; (b) $\chi(y')$; and (c) $\chi(y')'$. The ratios are shown through $n=14$. The solid lines are the asymptotic behavior of the ratios expected for $\alpha'=0.0$.

for the other functions.

For $\chi^{\dagger}(y', \phi)$ we obtain very good ratios in the range $x \simeq 1.5$ to 3.5. In this range of x, ratios for the function $[\chi^{\dagger}(y', \phi)]^{4/7}$ are independent of n and ϕ being similar to those shown in Fig. 7. These results are consistent with the conjecture

$$\gamma' = \tfrac{7}{4} \tag{54}$$

along the second-order line.

For $R(y', \phi)$ we have the estimate of Gaunt and Fisher that at $x=1$, $\beta = \frac{1}{8}$. The function $[R(y', \phi)']^{8/7}$ gives ratios that are independent of n and ϕ over the range $x=1.5$ to 6.0. For $x > 6.0$, the ratios begin to drift apart as a function of ϕ. Thus we estimate that along the second-order line

$$\beta = \tfrac{1}{8} . \tag{55}$$

Figure 9 shows the ratios for $\rho(y', \phi)$, $\chi(y', \phi)$, and $\chi(y', \phi)'$ for $x=1.0$ and $\phi=3.0$ using the 14-term high-density series given in Ref. 1. The straight lines are plots of $r'_n = r_n - \phi$ with r_n given by Eq. (42b) for $\alpha = 0.0$ (logarithmic singularity). The data of Fig. 9 support the conjecture that

$$\chi(y') \sim -\ln(y'_\sigma - y') . \tag{56}$$

Note that

$$y'_\sigma = 1/y_\sigma . \tag{57}$$

Thus the intercept in Fig. 9 is $(y'_\sigma)^{-1} = y_\sigma = 3.76$ confirming nicely the estimate of Gaunt and Fisher at $x=1.0$.

We note that the ratios of Fig. 9 were obtained using $\phi = 3.0$, while most of the other ratio plots we have shown are for ϕ in the range 0.5 to 1.5. From Eq. (40) one sees that the characteristic variable in $r_n(\phi)$ is ϕy_σ. In the Ising model and the present model for $x > 2$, $y_\sigma \simeq 1$ and we use ϕ such that $\phi y_\sigma \simeq 1$. At $x=1.0$, $y_\sigma \simeq 3.8$ and y'_σ

$\simeq 1/3.8$; in the high-density series the variable that occurs in Eq. (40) is $\phi y_\sigma'$. Thus using $\phi = 3.0$ again gives $\phi y_\sigma' \simeq 1$. We note that, in general, the range of ϕ that is appropriate is determined by y_σ or y_σ'.

One of the major problems in the analysis of the behavior of the present model has been to decide when not to accept the results of ratio plots or Padé approximants. We wish to conclude this section on the analysis of series by giving another example of a poorly converged series. We will use as our example the temperature dependence of the ratios for $\chi(y', \phi)$. From Fig. 9 we note that the ratios support the conjecture that at $x = 1.0$, $\alpha' = 0.0$ (in Fig. 9, the middle curve is for χ). One obtains the same behavior down to about $x \simeq 1.3$ and we conjecture that $\alpha' = 0.0$ all along the second-order line. Figure 5 shows the ratios for $\chi(y', \phi)$ at $x = 6.0$ and here $\alpha_t' \simeq 1.00$. It is of course impossible for the beginning terms of a series (which are finite polynomials in x) to exhibit an abrupt change such as α' changing from $\alpha' = 0.0$ along the second-order line to $\alpha_t' = 1.0$ at the TCP. Thus what one observes is a gradual change in character in the beginning terms of a series, for example, from that shown in Fig. 5 to that shown in Fig. 9. Figure 10 shows the ratios for $\chi(y', \phi)$ and $\chi(y', \phi)'$ at $x = 2.0$ for $\phi = 0.5$, 1.0, and 1.5. From the ratios for $[R(y', \phi)']^{8/7}$ which converge well at $x = 2.0$, we know that the intercept is at the star shown in Fig. 10 at $1/n = 0.0$. The data of Fig. 10 indicate clearly how misleading the ratios can be, especially if one had only the beginning terms. Consider the case if one had only the ratios covering the straight-line portion shown in Fig. 10; if one used only a single value of ϕ, one would conclude that the ratios gave a very good linear plot and one would obtain therefrom completely erroneous values of y_σ' and α.

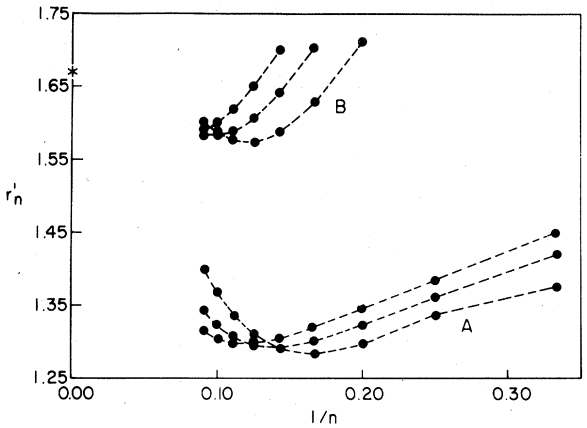

FIG. 10. Ratios r_n' at $x = 2.0$ for (a) $\chi(y')^{15/14}$; (b) $[\chi(y')']^{15/14}$. Each set of curves is for $\phi = 0.5$, 1.0, and 1.5. The star at $1/n = 0$ indicates the actual values of y_σ^{-1}. The ratios are shown through $n = 11$.

V. PHASE DIAGRAM

A. Density series

Gaunt and Fisher[11] found that at $x = 1.0$ $\chi^\dagger(\rho)$ gave smoothly varying ratios yielding $\rho_\sigma \simeq 0.37$ as the radius of convergence. For x greater than about 1.2 none of the $S(\rho, \phi)$ give smoothly varying ratios and the Padé approximants are very irregular. It is disappointing that the density series do not yield $\rho_\sigma(x)$. One can only hope that perhaps some form of transformation of the series other than the Euler transform will give useful results. But we have been unsuccessful in obtaining any useful information from density series for $x > 1$.

B. Numerical isotherms

While the analysis of density series with respect to obtaining ρ_σ and exponents was unfruitful, numerical Padé approximants to $\beta p(\rho)$ do yield an estimate of ρ_σ from the intersection of the low- and high-density series. Figure 11 shows the diagonal Padé approximant to $\beta p(\rho)$ using 10-term high- and low-density virial series as a function of x. In the range $x = 1.0$ to $x = 2.5$ the high- and low-density isotherms doubly intersect. At $x = 1.0$,

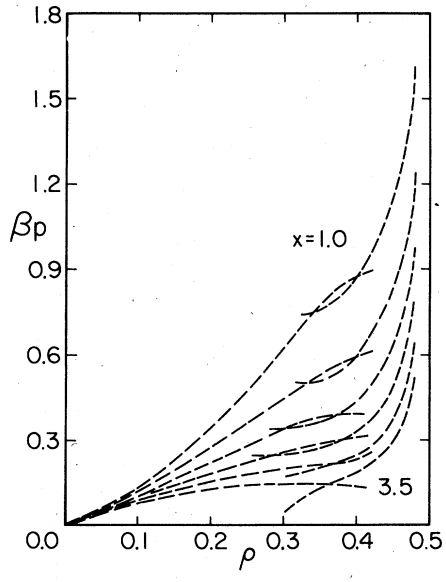

FIG. 11. Diagonal Padé approximants to $\beta p(\rho)$ using ten term low- and high-density virial series. The pairs of curves are, from top to bottom, for $x = 1.0$ to $x = 3.5$ in increments of 0.5. In the range $x = 1.0$ to $x = 2.5$ the low- and high-density approximants doubly intersect.

the midpoint of the double intersection agrees with $\rho_\sigma \simeq 0.37$ obtained from ratios for $\chi^\dagger(\rho)$. For $x=1.0$ to 2.5 in increments of 0.5, the midpoint of the double intersection occurs at $\rho_\sigma \simeq 0.37$, 0.36, 0.34, and 0.32, respectively, giving an estimate of the variation of the second-order line ρ_σ with temperature (x). For $x>3$ one does not obtain a double intersection, presumably due to poor convergence and the fact that one is approaching x_{TCP} below which the transition densities differ on the high- and low-density sides.

C. Extrapolation of activity series

For $x>3.5$ the partial series

$$\beta p(m)=\sum_{n=1}^{m} b_n z^n, \quad \rho(m)=\sum_{n=1}^{m} n b_n z^n \tag{58}$$

vary smoothly and monotonically with m when $\beta p(m)$ and $\rho(m)$ are plotted versus $1/m$. This is true of both the high- and low-density activity series. Fitting the $\beta p(m)$ to a polynomial in $1/m$ and calculating $\beta p(1/m=0)$ one can obtain an estimate of z_σ from the intersection of the high- and low-density isotherms. One can obtain the transition density by differentiating the polynomial for $\beta p(z)$ or by fitting $\rho(m)$ to a polynomial in $1/m$; the two methods give the same transition density to within 1%.

Using the data from Fig. 11 for $\rho_\sigma(x)$ along the second-order line and the slopes at the intersection of extrapolated high- and low-density activity series for βp for $\rho_\sigma(x)$ for $x>3.5$, we obtain an approximate phase diagram as shown in Fig. 12.

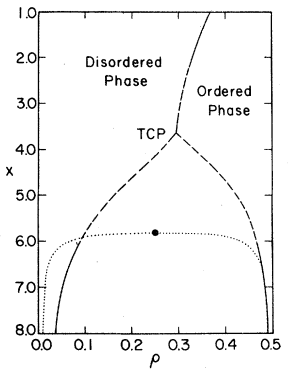

FIG. 12. Phase diagram for the present lattice gas. The upper solid line gives the second-order line as determined from the data of Fig. 11. The lower solid lines indicate the first-order lines as determined from the extrapolation of activity series for βp; the dashed curve indicates the portion of the diagram where the convergence of the extrapolation procedure is in doubt. The dotted curve gives the coexistence curve for the two-dimensional Ising model; the dot is the Ising model critical point.

In Fig. 12, the portions of $\rho_\sigma(x)$ that we have the highest confidence in are given by solid lines. These portions include the second-order line from $x=1.0$ to $x=2.5$ and the first-order lines for $x>6$. The dashed portion of the first-order lines we have less confidence in; one notes that the first-order lines meet the extrapolation of the second-order line at the following point

$$x_{\mathrm{TCP}} \simeq 3.65, \quad \rho_{\mathrm{TCP}} \simeq 0.29 . \tag{59}$$

The reason we do not have great confidence in the dashed portion of the first-order lines is that when one applies the same extrapolation procedure to the two-dimensional Ising model, one obtains the coexistence curve quite accurately for $x>6.5$, but one misses the true critical point at $x_c=5.828$, the two first-order lines coming together at $x \sim 4.0$. For comparison, the two-dimensional Ising model coexistence curve is shown by the dotted curve (interpreting the density scale as varying from zero to the maximum possible density). Thus at low temperature, the extrapolation of activity series is quite accurate, but for the Ising model in the neighborhood of x_c, the convergence is quite slow. Since the extrapolation procedure to obtain the first-order lines for the Ising model overestimates the critical temperature, we conjecture that x_{TCP} of Eq. (59) is an underestimate and that ρ_{TCP} is an overestimate.

Runnels, Salvant, and Streiffer[13] have estimated the transition densities for the present model by extrapolating data obtained for lattice strips of finite width (or diameter, since they use periodic boundary conditions). Their Fig. 4 is qualitatively similar to our Fig. 12, the main difference being that their diagram has the shape of a λ transition, the first-order lines asymptotically coming together in a cusp. They estimate the value of x at which the first-order lines finally meet as $x_{\mathrm{TCP}} \simeq e^{0.4}=1.49$. From our experience in the present work with extrapolating partial series for βp, we find for both the Ising model and the present model that the partial series extrapolate very smoothly. The problem is that for the Ising model in the neighborhood of x_c, the extrapolation completely misses the true critical point, giving, as mentioned previously, $x_c \sim 4$ as the point where the first-order lines come together.

Kaye and Burley,[14] using a Kikuchi approximation applied to the present model, find $x_{\mathrm{TCP}} = e^{1.05}=2.86$. This value is considerably larger than the estimate of Runnels *et al.*,[13] but smaller than our estimate of the upper limit given in Eq. (59).

It is clear that the central remaining problem

concerning the present model is an accurate determination of x_{TCP}.

VI. PHASE-TRANSITON BEHAVIOR

An understanding of the behavior of the present model centers around the sublattice structure illustrated in Fig. 2(b). In brief review, at low densities both sublattices are equally favored and one has a system that resembles a gas or a fluid above the critical point with no long-range order. At very high densities most of the particles will exist on only one of the sublattices (at close packing all of the particles are on one sublattice), the nearest-neighbor exclusion forcing alternate sites to be occupied. Figure 2(b) illustrates a high-density configuration of particles where all of the particles are on one sublattice except one near the center. The high-density phase can thus be viewed as the lattice-model analog of a solid with long-range order (favoring of one sublattice). As the density is decreased from close packing ($\rho=\frac{1}{2}$), particles are first removed from the dominant sublattice; as enough holes are created on the dominant sublattice, it becomes possible for particles to become "unlocked" from the dominant sublattice and form small islands of particles on the other sublattice (Gaunt and Fisher[11] use the analogy of islands breaking away from the mainland). This migration from the dominant sublattice is graphically illustrated in the high-density series given in the Appendix where one can see precisely how many particles can exist on the nondominant sublattice (taken as the B sublattice) as a function of the number of particles removed from the system. Thus the present model is the lattice-model analog of the gas-solid transition in contrast with the Ising model which is an analog of the gas-liquid transition. At the conclusion of this section we will return to the question of lattice models that are analogs of the complete gas-liquid-solid system.

From the above comments it is clear that the sublattice structure of the present model is crucially important in determining its behavior. One gains considerably insight into the present model by introducing a parameter (the "staggered activity") that measures the difference between the activities of the two sublattices

$$z_{st}=z_a/z_b\,. \tag{60}$$

Our discussion then is with reference to a three-dimensional thermodynamic field space (x, z, z_{st}) rather than the two-dimensional field space (x, z).[20]

For a lattice gas $z_{st}=1$ since one has no way of making one sublattice favored over another. If the present model were used to treat surface adsorption where there were indeed different alternating binding sites, then $z_{st}\neq 1$, but one could not manipulate this variable experimentally at will. For certain magnetic systems the magnetic field analog of z_{st} would be a variable under experimental control. Thus the introduction of the z_{st} dimension in the thermodynamic field space for the lattice gas is to be viewed as a mathematical construction that gives additional insight into the behavior of the model, the real world being represented by $z_{st}=1$.

If z_{st} is turned on (made larger than 1) the A sublattice will be favored for the occupation of particles over the B sublattice for $z>z_\sigma$. Likewise if z_{st} is turned off (made smaller than 1) most of the particles will occupy the B sublattice. Figure 13 schematically shows the coexistence surfaces for the present model in the space (x, z, z_{st}). The descending dashed curve in the x-z plane represents $z_\sigma(x)$ (as given in Fig. 8; $y_\sigma=z_\sigma x^2$). The shaded surface in the x-z plane above $z_\sigma(x)$ is a coexistence or first-order phase-transition surface. The two coexisting phases are the phases dominated by occupancy of the A or B sublattice depending on whether z_{st} is greater or lesser than 1. These two phases are related by symmetry $[\rho_A(x, z_{st})=\rho_B(x, 1/z_{st})]$ and will have the same chemical potential at $z_{st}=1$.

From the above point of view as the system

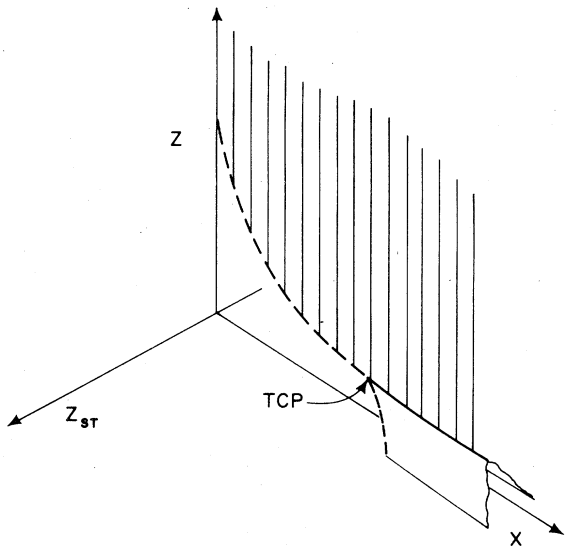

FIG. 13. Coexistence surfaces for the present model in (x,z,z_{st}) space. The shaded area represents the region where the A and B sublattice phases are in equilibrium. The A or B sublattice phases are in equilibrium in the "wings" (sides of the "tent") with the disordered phase. The origin of the z_{st} axis is at $z_{st}=1$.

passes through a second-order phase transition point from the ordered phase ($z > z_\sigma, z_{st}=1$) the A and B sublattice phases become identical and hence the line of second-order points is more correctly looked upon as a line of critical points.

The A and B sublattice phases can be stabilized for $z < z_\sigma$ if z_{st} is made different from unity. This accounts for the "wings" in Fig. 13. The wings are first-order coexistence surfaces with either the A or B sublattice phases being in equilibrium with the disordered phase. The line of first-order phase-transition points is actually then a line of triple points with the A and B sublattice phases and the disordered phase coexisting. The significance of the point at which the transition changes from second order now becomes clear. At this point three phases become identical simultaneously and hence this point is a tricritical point. Tricritical points have been found in a number of systems including ^{3}He-^{4}He mixtures, magnets, three- and four-component fluids, and NH_4CI.[21]

Having discussed the general nature of the phase transition behavior, we turn now to a discussion of the divergences of the thermodynamic parameters along the first- and second-order phase-transition lines.

In the Ising model the critical exponents can be classified according to the path of approach to the critical point and the direction of the derivative involved relative to the coexistence curve. Following Griffiths and Wheeler,[20] one can distinguish between paths that are parallel or perpendicular to the coexistence curve $[y_\sigma(x)]$. Quantities such as K_T which are second derivatives of the chemical potential in directions not parallel diverge strongly at the critical point while quantities such as C_V which are second derivatives of the chemical potential taken parallel to the coexistence curve diverge weakly. For example, in the two-dimensional Ising model

$$K_T \sim (T - T_c)^{-7/4}, \quad C_V \sim -\ln(T - T_c) \tag{61}$$

for $T > T_c$ along the critical isochore.

As illustrated in Fig. 13, in the present model one has a coexistence surface. Since

$$\chi = \partial^2\Gamma/\partial(\ln z)^2, \qquad \chi^\dagger = \partial^2\Gamma/\partial(\ln z_{st})^2, \tag{62}$$

one sees that χ is a derivative in the direction parallel to the coexistence curve while $\chi^\dagger$ is a derivative in the perpendicular direction. Thus one expects that $\chi^\dagger$ will diverge strongly and χ weakly at the line of critical points (second-order line). Invoking current ideas on universality[22] and smoothness[23] one in fact would expect

$$\alpha = \alpha' = 0 \ \text{(logarithmic singularity)}, \quad \gamma = \gamma' = \tfrac{7}{4}, \quad \beta = \tfrac{1}{8}, \quad \alpha + 2\beta + \gamma = 2. \tag{63}$$

Further evidence for the truth of such a conjecture is Fisher's result of $\beta = \frac{1}{8}$ and $\alpha = 0$ exactly for his superexchange lattice gas[24] (this model has half the bonds of the present model with the same hard core; Fisher's exact solution is for the isotherm $x = 2$).

At the tricritical point one has the renormalization-group ϵ expansion of Stephens and McCauley[25] who find

$$\alpha_t = \tfrac{1}{2} + 1/2\epsilon + \cdots, \tag{64}$$

where $\epsilon = d - 3$. Hence for $d = 2$

$$\alpha_t \simeq 1.0. \tag{65}$$

In the present work we find that the ratios for the series presented in Table I are asymptotically independent of n and ϕ.

Our results outlined in Table I support the values for the exponents given in Eqs. (63) and (65). We emphasize that the problems we have outlined concerning the analysis of activity series (loss of convergence outside of certain ranges of x, lack of a precise value for x_{TCP}, and the possibility of an essential singularity for $x > x_{TCP}$) preclude, in our view, any stronger statement concerning the values of the exponents. As an example, we refer back to Fig. 5. For the two-dimensional Ising model along the critical isotherm

$$\chi \sim (y'_\sigma - y')^{-14/15}. \tag{66}$$

We initially guessed that since at low temperatures (in the neighborhood of $x = 4$ to 5) the series for the present model behaved in a similar fashion to the series for the Ising model that one would have $\alpha'_t = \frac{14}{15} = 0.934$. Figure 5 shows the

TABLE I. Summary of functions used.

Function	Temperature range	No. of terms in series
	Low density	
$\chi(y, \phi)$	$x \cong 3.7$ to 5.0	11
$[\chi^\dagger(y, \phi)]^{4/7}$	$x \cong 1.3$ to 1.8	9
$[\chi_e^\dagger(y, \phi)]^{4/7}$	$x \cong 2.0$ to 3.9	9
$\chi^\dagger(y, \phi)$	$x \cong 5.0$ to 6.0	9
	High density	
$\chi(y', \phi)'$	$x \simeq 1.0$ to 1.3	14 at $x = 1$ 11 for $x > 1$
$\chi(y', \phi)$	$x \simeq 5.0$ to 6.0	11
$[\chi^\dagger(y', \phi)]^{4/7}$	$x \simeq 1.5$ to 3.5	8
$[R(y', \phi)']^{8/7}$	$x \simeq 1.5$ to 6.0	8

ratios for $\chi(y', \phi)^{15/14}$ and one obtains points that are independent of n and ϕ. On the other hand the ϵ expansion of Eq. (64) predicts $\alpha_t' \simeq 1.0$. As we have discussed in connection with the data of (49), our lack of knowledge of x_{TCP} does not let us distinguish between $\alpha_t' = \frac{14}{15}$ and $\alpha_t' = 1.0$. Our data thus support any prediction that $\alpha_t' \simeq 1.00 \pm 0.05$. This kind of analysis of series can then clearly tell the difference between the exponents 0.0, 1.0, and 1.75 (in the ranges of x where the series are well converged), the general confidence limit on a particular exponent being about ± 0.1 and in some cases quite a bit better.

For the exponents at the tricritical point we find $\alpha_t \simeq 1.0$ and $\gamma_t \simeq 1.0$. We do not see any change in β from $\beta \simeq \frac{1}{8}$ down to about $x = 6.0$. The uncertainties in α_t and γ_t (due largely to the uncertainty in the value of x_{TCP}) are such that these results do not imply a violation of the scaling law $\alpha_t + 2\beta_t + \gamma_t = 2$. From a computer simulation for the two-dimensional spin-1 Ising model, Arora and Landau[26] found $\beta_t \simeq 0.09$ and $\gamma_t \simeq 1.0$.

We conclude with some comments on the relation of the present model to the general question of a gas-liquid-solid system.

Lattice models can be viewed as a construct used to approximate the multidimensional configuration integral in continuous space, a degree of realism being traded for high precision in obtaining series and hence detailed knowledge of the nature of the singularities associated with phase transitions. And the close agreement between experimental critical exponents and those obtained from the three-dimensional Ising model supports the idea that the discretization of space does not lead to results that have no connection with the real world. One anticipates that as one makes a lattice of finer and finer grid that lattice models would approach the continuous space limit more closely. The present model can be viewed as the first step in this direction as illustrated by Figs. 2(a) and 2(b), the present model being an increase by a factor of 2 in the number of lattice points keeping the particle size constant. The interesting feature of the present model is that by increasing the density of lattice sites over the two-dimensional Ising model one has not improved the degree to which the present model describes a gas-liquid critical point, but one has changed qualitatively the nature of the transition, the extended hard-core repulsion introducing an ordering effect making the present model represent a gas-solid system.

There is evidence[27] that by introducing an extended region of attractive sites around each particle one can produce a lattice model that includes the gas, liquid, and solid phases, the simple idea being that one must have the possibility of low-energy configurations that do not necessarily lead to a regular arrangement of the particles in order to produce the liquid phase. Since high-temperature series are expansions about the independent-particle state, such expansions are not possible for systems containing an extended hard core. Hence the most detailed knowledge of singularities in such systems, in lieu of exact solutions, must come from the analysis of activity series. The present work illustrates both the difficulties and the positive results to be encountered in such an approach that hopefully can be applied in the future to a model exhibiting full three-phase behavior.

ACKNOWLEDGMENT

This work was supported in part by a Camille and Henry Dreyfus Foundation Grant to one of the authors (D.P.).

APPENDIX: SUBLATTICE ACTIVITY SERIES

In this Appendix we give exact low- and high-density series expansions in the sublattice activities as defined by Eqs. (4a) and (4b). For a given value of n, if one sums the b_{mn} and b'_{mn} over m one obtains, respectively, the b_n and b'_n previously published.[1] The asterisks on the terms in b_9 indicate that we are uncertain to ± 1 in the last digit for the terms indicated (one obtains the coefficients by solving simultaneous equations in two variables, z_b and x and the uncertainty arises from having reached the computer's limit of accuracy).

For the low-density series we give only those terms that cannot be determined by the symmetry relation $b_{mn} = b_{n-m,m}$.

A. Low-density series

$$b_{01} = \tfrac{1}{2};\quad b_{02} = -1\tfrac{1}{4} + x;\quad b_{12} = -2;\quad b_{03} = 5\tfrac{1}{6} - 8x + 3x^2.$$

$$b_{13} = 11 - 6x;\quad b_{04} = -26\tfrac{1}{8} + 59x - 42\tfrac{1}{2}x^2 + 9x^3 + \tfrac{1}{2}x^4.$$

$$b_{14} = -70 + 84x - 24x^2;\quad b_{24} = -91 + 76x - 17x^2.$$

$$b_{05} = 147\tfrac{3}{5} - 436x + 463x^2 - 200x^3 + 21\tfrac{1}{2}x^4 + 4x^5.$$

$$b_{15} = 478 - 894x + 528x^2 - 90x^3 - 4\tfrac{1}{2}x^4.$$

$$b_{25} = 760 - 1006x + 442x^2 - 66x^3.$$

$$b_{06} = -894\tfrac{11}{12} + 3260x - 4572x^2 + 2996\tfrac{1}{3}x^3 - 825\tfrac{1}{2}x^4 + 15x^5 + 20x^6 + x^7.$$

$$b_{16} = -3402 + 8656x - 7864x^2 + 2876x^3 - 250x^4 - 44x^5.$$

$$b_{26} = -6388 + 12\,058x - 8208x^2 + 2352x^3 - 208\tfrac{1}{2}x^4 - 12x^5.$$

$$b_{36} = -7726\tfrac{2}{3} + 12\,912x - 8176x^2 + 2320x^3 - 250x^4 .$$

$$b_{07} = 5698\tfrac{4}{7} - 24\,664x + 42\,977x^2 - 37\,820x^3 + 16\,804\tfrac{1}{2} - 2832x^5 - 243x^6 + 68x^7 + 11x^8 .$$

$$b_{17} = 24\,883 - 80\,120x + 98\,832x^2 - 56\,582x^3 + 13\,415x^4 - 114x^5 - 260x^6 - 12x^7 .$$

$$b_{27} = 53\,861 - 134\,002x + 127\,168x^2 - 56\,324x^3 + 10\,743x^4 - 262x^5 - 116x^6 .$$

$$b_{37} = 75\,997 - 161\,698x + 136\,457x^2 - 56\,654x^3 + 11\,215\tfrac{1}{2}x^4 - 684x^5 - 45x^6 .$$

$$b_{08} = -37\,619\tfrac{1}{16} + 188\,520x - 392\,545\tfrac{1}{2}x^2 + 433\,835x^3 - 266098\tfrac{1}{4}x^4 + 82\,395x^5 - 6661\tfrac{1}{2}x^6 - 1993x^7 + 97\tfrac{1}{4}x^8 + 67x^9 + 3x^{10} .$$

$$b_{18} = -185\,568 + 722\,976x - 1\,129\,806x^2 + 887\,328x^3 - 348\,986x^4 + 50\,560x^5 + 4590x^6 - 1000x^7 - 154x^8 .$$

$$b_{28} = -454\,809 + 1\,414\,028x - 1\,747\,948x^2 + 1\,078\,599x^3 - 332\,964x^4 + 38\,732x^5 + 2489x^6 - 571x^7 - 31x^8 .$$

$$b_{38} = -731\,550 + 1\,935\,112x - 2\,083\,924x^2 + 1\,159\,368x^3 - 341\,664x^4 + 44\,912x^5 + 94x^6 - 428x^7 .$$

$$b_{48} = -849\,844\tfrac{1}{2} + 2\,118\,240x - 2\,188\,821x^2 + 1\,188\,700x^3 - 349\,205\tfrac{1}{2}x^4 + 47\,962x^5 - 707x^6 - 324x^7 - 8x^8 .$$

$$b_{09} = 255\,304\tfrac{13}{18} - 1\,453\,478x + 3\,520\,021x^2 - 4\,683\,826\tfrac{2}{3}x^3 + 3\,665\,016\tfrac{1}{2}x^4 - 1\,641\,164x^5 + 345\,867x^6 + 2556x^7 - 9893x^8 - 710x^9 + 270x^{10} + 36x^{11} + \tfrac{1}{2}x^{12}$$

$$b_{19} = 1\,404\,147 - 6\,420\,508x + 12\,163\,116x^2 - 12\,185\,366x^3 + 6\,738\,644x^4 - 1\,859\,290x^5 + 122\,277x^6 + 39\,524x^7 - 1344\tfrac{1}{2}x^8 - 1072x^9 - 45x^{10}$$

$$b_{29} = 3\,843\,004 - 14\,385\,886x + 22\,095\,878x^2 - 17\,765\,220x^3 + 7\,799\,767x^4 - 1\,685\,656x^5 + 80\,214x^6 + 24\,494x^7 - 985x^8 - 396x^9 .$$

$$b_{39} = 6\,931\,858\tfrac{2}{3} - 22\,186\,946x + 29\,518\,860x^2 - 20\,975\,906x^3 + 8\,409\,747x^4 - 1\,776\,160x^5 + 125\,204x^6 + 15\,358^*x^7 - 1820x^8 - 114x^9 .$$

$$b_{49} = 9\,130\,744 - 26\,784\,398x + 33\,296\,381x^2 - 22\,549\,022x^3 + 8\,809\,948x^4 - 1\,875\,032x^5 + 151\,361^*x^6 + 11\,940^*x^7 - 1919\tfrac{1}{2}^*x^8 - 76^*x^9 .$$

B. High-density series

$$b'_{01} = 1;\quad b'_{02} = 2\tfrac{1}{2} + 2x;\quad b'_{03} = 10\tfrac{1}{3} - 16x + 6x^2;\quad b'_{13} = 1 .$$

$$b'_{04} = -52\tfrac{1}{4} + 118x - 85x^2 + 18x^3 + x^4 ;$$

$$b'_{14} = -12 + 8x;\quad b'_{24} = 2 .$$

$$b'_{05} = 295\tfrac{1}{5} - 872x + 926x^2 - 400x^3 + 43x^4 + 8x^5 .$$

$$b'_{15} = 110 - 144x + 40x^2 + 4x^3;\quad b'_{25} = -30 + 20x ;$$

$$b'_{35} = 6;\quad b'_{45} = 1 .$$

$$b'_{06} = -1789\tfrac{5}{6} + 6520x - 9144x^2 + 5992\tfrac{2}{3}x^3 - 1651x^4 + 30x^5 + 40x^6 + 2x^7 .$$

$$b'_{16} = -928 + 1816x - 1056x^2 + 104x^3 + 44x^4 ;$$

$$b'_{26} = 309\tfrac{1}{2} - 418x + 120x^2 + 12x^3 ;$$

$$b'_{36} = -108 + 64x + 4x^3 .$$

$$b'_{46} = -3 + 12x;\quad b'_{56} = 8;\quad b'_{66} = 2 .$$

$$b'_{07} = 11\,397\tfrac{1}{7} - 49\,328x + 85\,954x^2 - 75\,640x^3 + 33\,609x^4 - 5664x^5 - 486x^6 + 136x^7 + 22x^8 .$$

$$b'_{17} = 7580 - 19\,800x + 17\,798x^2 - 5540x^3 - 289x^4 + 268x^5 + 18x^6 .$$

$$b'_{27} = -2742 + 5656x - 3448x^2 + 372x^3 + 138x^4 + 4x^5 .$$

$$b'_{37} = 1254 - 1544x + 328x^2 + 88x^3 .$$

$$b'_{47} = -97 - 122x + 102x^2 + 8x^3 ;$$

$$b'_{57} = -137 + 100x + 8x^2 .$$

$$b'_{67} = -12 + 28x;\quad b'_{77} = 22 ;$$

$$b'_{87} = 6;\quad b'_{97} = 1 .$$

$$b'_{08} = -75\,238\tfrac{1}{8} + 377\,040x - 785\,091x^2 + 867\,670x^3 - 532\,196\tfrac{1}{2}x^4 + 164\,790x^5 - 13\,323x^6 - 3986x^7 + 194\tfrac{1}{2}x^8 + 134x^9 + 6x^{10} .$$

$$b'_{18} = -61\,072 + 199\,896x - 244\,580x^2 + 129\,336x^3 - 19\,260x^4 - 5560x^5 + 963x^6 + 216x^7 + 4x^8 .$$

$$b'_{28} = 22\,404 - 62\,906x + 60\,148x^2 - 19\,960x^3 - 724x^4 + 858x^5 + 102x^6 .$$

$$b'_{38} = -11\,976 + 22\,920x - 12\,052x^2 + 48x^3 + 804x^4 + 48x^5 .$$

$b'_{48}=1781-350x-1828x^2+622x^3+116x^4+4x^5$.

$b'_{58}=1508-2312x+588x^2+176x^3$.

$b'_{68}=-80-358x+282x^2+20x^3$;

$b'_{78}=-468+312x+28x^2$.

$b'_{88}=-51+92x+4x^2$; $b'_{98}=40+16x$.

$b'_{10,8}=30$; $b'_{11,8}=8$; $b'_{12,8}=2$.

[1]M. W. Springgate and D. Poland, J. Chem. Phys. 62, 680 (1975).
[2]C. Domb, Nuovo Cimento Suppl. 1 9, 9 (1958).
[3]H. N. V. Temperly, Proc. Phys. Soc. London 74, 183, 432 (1959); 77, 630 (1961); 80, 813, 823 (1962).
[4]D. M. Burley, Proc. Phys. Soc. London 75, 262 (1960).
[5]D. Levesque and L. Verlet, Phys. Lett. 11, 36 (1964).
[6]B. Jancovici and G. Stell, Physica 31, 1017 (1965).
[7]R. D. Kaye and D. M. Burley, Proc. Phys. Soc. 77, 451 (1965).
[8]L. K. Runnels and L. L. Combs, J. Chem. Phys. 43, 2840 (1965).
[9]F. H. Ree and D. A. Chesnut, J. Chem. Phys. 45, 3983 (1966).
[10]R. M. Nisbet and I. E. Farquhar, Physica 76, 259 (1974).
[11]D. S. Gaunt and M. E. Fisher, J. Chem. Phys. 43, 2840 (1965); D. S. Gaunt, J. Chem. Phys. 46, 3237 (1967).
[12]R. L. Dobrusin, Funct. Anal. Appl. 2, 292, 302 (1968).
[13]L. K. Runnels, J. P. Salvant, and H. R. Streiffer, J. Chem. Phys. 52, 2352 (1970).
[14]R. D. Kaye and D. M. Burley, J. Phys. A 7, 843 (1974).
[15]R. B. Griffiths, Phys. Rev. B 7, 545 (1973).
[16]H. E. Stanley, *Introduction to Phase Transitions and Critical Phenomena* (Oxford University, New York, 1971); Chap. 9.
[17]C. Domb and M. F. Sykes, J. Math. Phys. 2, 63 (1963).
[18]G. A. Baker, Jr., J. L. Gammel, and J. G. Willis, J. Math. Anal. Appl. 2, 405 (1961); D. L. Hunter and G. A. Baker, Jr., Phys. Rev. B 7, 3346 (1973).
[19]M. E. Fisher, Physica 3, 255 (1967).
[20]R. B. Griffiths and J. C. Wheeler, Phys. Rev. A 2, 1047 (1970).
[21]M. Blume, V. J. Emery, and R. B. Griffiths, Phys. Rev. A 4, 1071 (1971); D. M. Saul, M. Wortis, and D. Stauffer, Phys. Rev. B 11, 4964 (1974); F. Harbus and H. E. Stanley, Phys. Rev. B 8, 1141, 1156 (1973); B. Widom, J. Phys. Chem. 77, 2196 (1973).
[22]L. P. Kadanoff, in *Proceedings of the Enrico Fermi Summer School*, edited by M. S. Green (Academic, New York, 1971).
[23]R. B. Griffiths, Phys. Rev. Lett. 24, 1479 (1970).
[24]M. E. Fisher, J. Math. Phys. 4, 278 (1973).
[25]M. J. Stephens and D. McCauley, Physics Lett. A 44, 89 (1974).
[26]B. L. Arora and D. D. Landau, AIP Conf. Proc. 10, 870 (1973).
[27]J. Orban, J. Van Crean, and A. Bellemans, J. Chem. Phys. 49, 1778 (1968).